

Room acoustics simulation with single-leaf microperforated panel absorber using two-dimensional finite-element method

Takeshi Okuzono* and Kimihiro Sakagami

Environmental Acoustic Laboratory, Department of Architecture, Graduate School of Engineering, Kobe University, 1-1 Rokkodai-cho, Nada-ku, Kobe, 657-8501 Japan

(Received 11 December 2014, Accepted for publication 22 December 2014)

Keywords: Room acoustics simulation, Microperforated panel, Absorption modeling, Extended-reactive model, Surface impedance model

PACS number: 43.55.Ka, 43.55.Dt, 43.55.Ev [doi:10.1250/ast.36.358]

1. Introduction

Sound-absorbing materials play an important role in the control of acoustics in built environments. Recently, the development of absorbers using a microperforated panel (MPP), known as one of the next-generation sound-absorbing materials, is an area of active research because of its superior material properties. Various MPP absorbers and prediction methods of their absorption characteristics have been proposed [1,2]. Meanwhile, in the application of MPP absorbers to actual rooms, an accurate prediction method of sound fields in rooms with MPP absorbers by wave-based numerical methods such as the finite-element method (FEM) is necessary for full utilization of the absorption performance of MPP absorbers in room acoustical design. However, the development of such a prediction method is still incomplete.

To overcome this situation, the authors proposed a simple FE formulation in order to predict sound fields in rooms with MPP absorbers, and its validity was also presented through comparisons with electro acoustical equivalent circuit theory and wave theory in numerical experiments based on an impedance tube method [3,4]. Using the FEM, sound propagation inside a backing structure of an MPP absorber can be considered easily. However, in the previous studies i.e., Refs. [3,4], the application was limited to a one-dimensional sound field.

In this study, to further demonstrate the applicability of the presented FEM, a 2D room acoustics simulation with a single-leaf MPP absorber is performed, in which a surface impedance model based on a locally reactive assumption is also used for comparison. The effectiveness of the presented FEM is shown in comparison with results from the surface impedance model, focusing on the sound pressure level distribution in the room.

2. FE modeling of MPP absorber

2.1. Extended-reactive model

The presented FEM [3,4] can deal with sound propagation inside the backing structure of an MPP absorber. Therefore, in the present study, we define the absorption modeling of an MPP absorber by our method as extended-reactive modeling. Figure 1 shows an FE model of an MPP, in which $\Omega_{e,air}$ and

$\Gamma_{e,M}$ respectively represent the air element and the MPP element derived with contributions from both boundary surfaces of the MPP: $\Gamma_{e,Ma}$ and $\Gamma_{e,Mb}$. p_a and p_b represent the sound pressures at the two sides of the MPP, respectively. v_f and v_m respectively represent the average particle velocity over the tube cross section and the vibration velocity of the MPP. \mathbf{n}_a and \mathbf{n}_b are the normal vectors at the boundaries. In this formulation, sound fields in the room and in the MPP absorber are connected through the following vibrating boundary conditions for both boundary surfaces of the MPP.

$$\frac{\partial p}{\partial n} = \begin{cases} -i\omega\rho_0(v_m + v_f) & \text{on } \Gamma_{e,Ma} \\ i\omega\rho_0(v_m + v_f) & \text{on } \Gamma_{e,Mb} \end{cases} \quad (1)$$

Here, i , ω , and ρ_0 respectively represent the imaginary unit, the angular frequency, and the air density. In Eq. (1), v_f and v_m can be calculated, respectively, from the definition of the acoustic impedance Z_M of the MPP and the equation of motion of the MPP as

$$Z_M = \frac{p_a - p_b}{v_f}, \quad (2)$$

$$i\omega M v_m = p_a - p_b. \quad (3)$$

Here, M is the surface density of the MPP. Only two material parameters, Z_M and M , are used in this formulation. For the present study, Z_M is calculated using Maa's impedance model [1].

2.2. Surface impedance model

This model uses the normal-incidence normalized acoustic impedance z_n on the surface of the MPP absorber under an impedance boundary condition based on the locally reactive assumption that neglects the incident-angle dependence of the normalized acoustic impedance. For the present study, z_n for a single-leaf MPP absorber can be obtained on the basis of electro acoustical equivalent circuit theory [5]. According to the theory, the oblique incidence surface impedance z_θ is given as

$$z_\theta = \left(\frac{\rho_0 c_0}{Z_M} + \frac{\rho_0 c_0}{i\omega M} \right)^{-1} \cos \theta - i \cot(k_0 L \cos \theta), \quad (4)$$

where c_0 , k_0 , and L respectively represent the speed of sound, the wave number, and the length of the air cavity. Therefore, z_n is calculated by setting $\theta = 0$.

*e-mail: okuzono@port.kobe-u.ac.jp

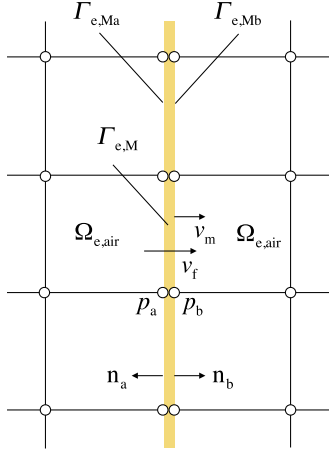


Fig. 1 An FE model of an MPP.

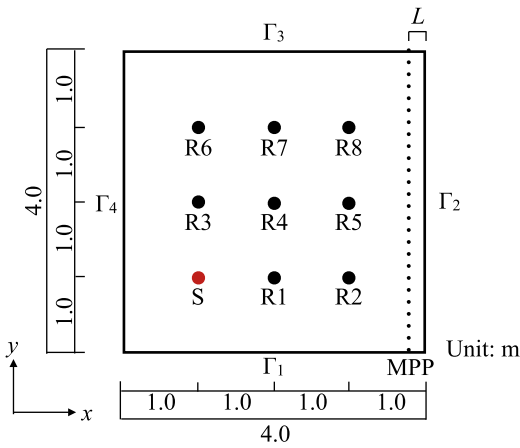


Fig. 2 Sound field with the single-leaf MPP absorber to be analyzed.

3. Numerical experiments

3.1. Setup of FE analysis

To show the effectiveness of the presented extended-reactive model, a two-dimensional sound field with a single-leaf MPP absorber, as shown in Fig. 2, is analyzed at frequencies from 56 Hz to 1,123 Hz with 1 Hz intervals, using the extended-reactive model and the surface impedance model. The results are compared with results obtained without the single-leaf MPP absorber in the 1/3-octave-band mean sound pressure level (SPL) and in the 1/3-octave-band SPL distribution. The 1/3-octave-band mean SPL is calculated from sound pressures at receiving points R1 to R8. In Fig. 2, Γ_2 is a rigid boundary and the remaining boundaries are absorbing boundaries with a real-valued finite impedance that corresponds to a statistical absorption coefficient of 0.092. An MPP is placed in front of the rigid boundary with an air cavity between them ($x = 4.0 - L$ m, $y = 0.0 - 4.0$ m). The material parameters of the MPP are $d = t = 0.144$ mm, $\sigma = 0.52\%$, and $M = 2.0$ kg/m², where d , t , and σ respectively represent the panel thickness, the hole diameter, and the perforation ratio. For the length of the air cavity, $L = 0.05$ m and 0.2 m

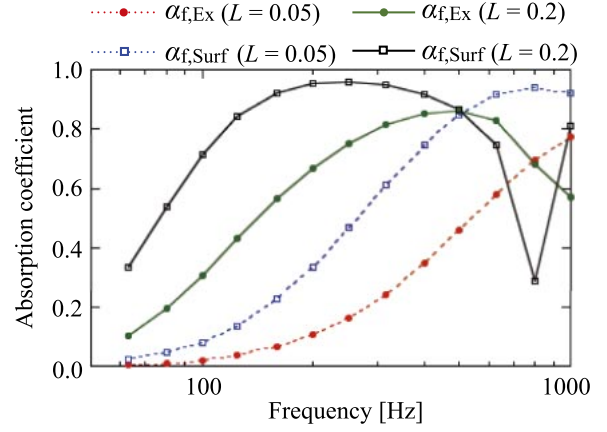


Fig. 3 Field incidence absorption coefficients obtained using extended-reactive model ($\alpha_{f,Ex}$) and surface impedance model ($\alpha_{f,Surf}$) for $L = 0.05$ m and 0.2 m.

are adopted. Note that the location of boundary Γ_2 in the surface impedance model is at $x = 4.0 - L$ m, which corresponds to the location of the MPP. As a sound source, a volume acceleration of $1.0 \text{ m}^3/\text{s}^2$ is given at point S. FE meshes of the extended-reactive model are created with 6,480 four-node quadrilateral FEs ($\Omega_{e,air}$: 6,400 and $\Gamma_{e,M}$: 80). In the surface impedance model, FE meshes are also created with 6,320 FEs ($L = 0.05$ m) and 6,080 FEs ($L = 0.2$ m) using four-node quadrilateral FEs. The spatial resolutions of the FE meshes are 6.1 elements per wavelength at the upper limit of the frequency. To reduce the dispersion error, the modified integration rule [6] is used for only the air elements.

3.2. Comparison of absorption characteristics of single-leaf MPP absorber between extended-reactive model and locally reactive model

Before presenting numerical results, we compare field incidence absorption coefficients obtained using the extended-reactive model and the surface impedance model. As presented previously, the oblique-incidence surface impedance z_θ of the single-leaf MPP absorber is given by Eq. (4). Therefore, by using the oblique-incidence absorption coefficient α_θ calculated from z_θ , the field incidence absorption coefficient α_f can be given as

$$\alpha_f = \frac{\int_{0^\circ}^{78^\circ} \alpha_\theta \sin \theta \cos \theta d\theta}{\int_{0^\circ}^{78^\circ} \sin \theta \cos \theta d\theta}. \quad (5)$$

The resulting α_f is called as the field incidence absorption coefficient in the extended-reactive model $\alpha_{f,Ex}$ because the incident angle dependence of the surface impedance is considered. On the other hand, the field incidence absorption coefficient in the surface impedance model $\alpha_{f,Surf}$ is also calculated using Eq. (5) with the assumption that z_n is independent of the incident angle.

Figure 3 shows $\alpha_{f,Ex}$ and $\alpha_{f,Surf}$ for the single-leaf MPP absorber with $L = 0.05$ m and 0.2 m. The $\alpha_{f,Surf}$ values are larger than the $\alpha_{f,Ex}$ values except at 630 Hz and 800 Hz in the case of $L = 0.2$ m. Also, $\alpha_{f,Surf}$ shows a deep dip at 800 Hz for

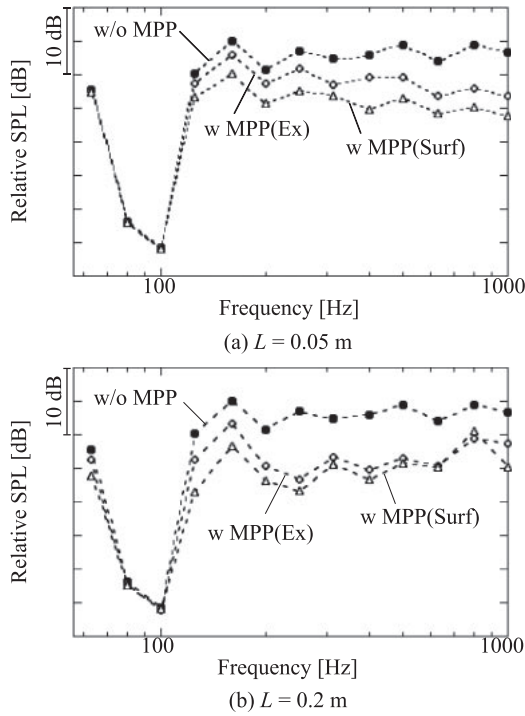


Fig. 4 Relative mean SPLs in room under three conditions of different lengths of the back cavity, (a) $L = 0.05$ m and (b) $L = 0.2$ m, where w/o MPP, w MPP(Ex), and w MPP(Surf) respectively represent the mean SPL without the MPP absorber, that obtained using extended-reactive model, and that obtained using surface impedance model.

$L = 0.2$ m, because α_θ for the extended-reactive model tends to have smaller values for a larger incident angle, whereas α_θ for the surface impedance model shows larger values with increasing incident angle. Furthermore, the frequency with a dip in α_θ in the case of the extended-reactive model shifts to a higher frequency with increasing incident angle, but that of the surface impedance model does not change, regardless of the incident angle.

From the results, it is expected that the reduction effect of the SPL after installing the single-leaf MPP absorber will be overestimated overall when using the surface impedance model in the following numerical results. Note that z_θ of Eq. (4) changes significantly with increasing incident angle, and both the acoustic resistance and the acoustic reactance have smaller values with increasing incident angle.

3.3. Results and discussion

First, relative mean SPLs in the room obtained using the extended-reactive model and the surface impedance model are compared with that obtained without the MPP absorber in Fig. 4(a) for $L = 0.05$ m and (b) for $L = 0.2$ m. As expected, overall, reductions of the mean SPLs when using the surface impedance model are larger than those when using the extended-reactive model at frequencies above 125 Hz, regardless of L . Also, the MPP absorber has a certain level of absorptivity at 80 Hz and 100 Hz for $L = 0.2$ m, but the reduction of the mean SPL cannot be observed at these frequencies, as shown in Fig. 4(b). This can be interpreted to

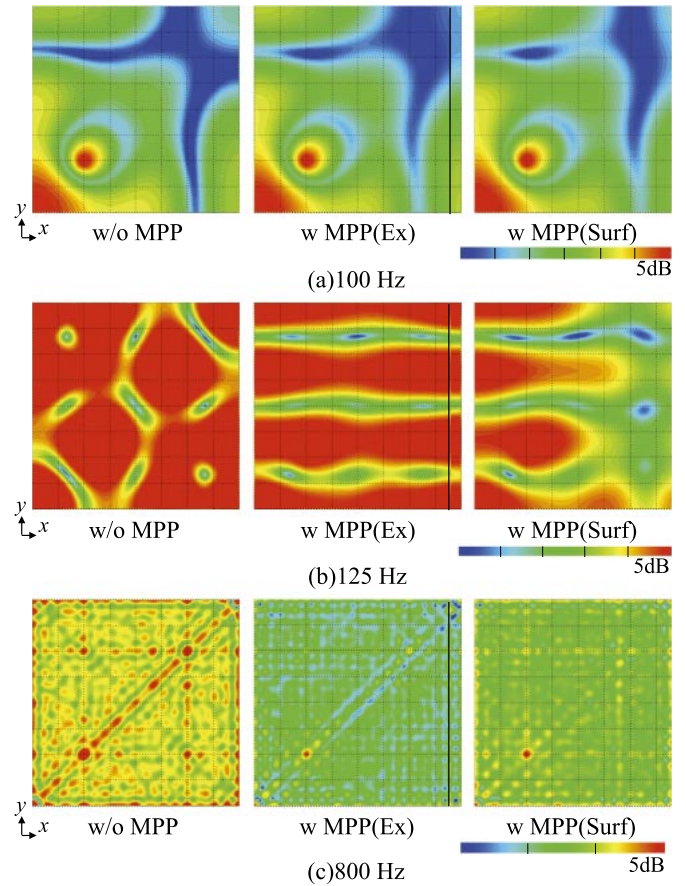


Fig. 5 SPL distributions in a room at (a) 100 Hz, (b) 125 Hz, and (c) 800 Hz, with $L = 0.2$ m, where w/o MPP, w MPP(Ex) and w MPP(Surf) respectively represent the SPL distribution without the MPP absorber, that obtained using extended-reactive model, and that obtained using surface impedance model.

mean that the MPP absorber that provides the Helmholtz resonance absorption does not function well at the frequency at which the dip occurs because the sound pressure is too low. In the result for 800 Hz with $L = 0.2$ m, it can also be seen that the mean SPL obtained using the extended-reactive model is lower than that obtained using the surface impedance model, where $\alpha_{f,\text{Surf}}$ has a deep dip.

Secondly, we present the difference in the SPL distributions in a room between the extended-reactive model and the surface impedance model. As representative cases of the results, Fig. 5 shows the SPL distributions at (a) 100 Hz, (b) 125 Hz, and (c) 800 Hz with $L = 0.2$ m. As mentioned previously, installing the MPP absorber has no effect at 100 Hz, and both the extended and locally reactive models yield similar SPL distributions as those without the absorber. At 125 Hz, on installing the MPP absorber, the SPL distribution changes significantly, and the axial wave along the y -axis dominates (Fig. 5(b)). Furthermore, the surface impedance model indicates a larger reduction of the SPL near the absorber. Meanwhile, at 800 Hz, which has a dip in $\alpha_{f,\text{Surf}}$, the SPL obtained using the surface impedance model is larger than that obtained using the extended-reactive

model, throughout the entire room. Note that although the results are omitted here, a difference in the SPL distributions between the two models is observed at frequencies above 125 Hz, regardless of L . These results revealed that the modeling of the single-leaf MPP absorber using the surface impedance model yields excessive attenuation in wide frequency ranges.

4. Conclusions

In this paper, we reported that the modeling of the backing cavity plays an important role in FE analysis for appropriately treating the incident angle dependence of the surface impedance of a single-leaf MPP absorber. For this purpose, the extended-reactive model using the presented FEM is useful and the effectiveness was shown through comparison with the surface impedance model.

Acknowledgment

This research was partially supported by a research grant from NIKKO Co., Ltd.

References

- [1] D. Y. Maa, "Microperforated-panel wideband absorbers," *Noise Control Eng. J.*, **29**(3), pp. 77–84 (1987).
- [2] K. Sakagami, M. Yairi and M. Morimoto, "Multiple-leaf sound absorbers with microperforated panels: An overview," *Acoust. Aust.*, **38**, 76–81 (2010).
- [3] T. Okuzono and K. Sakagami, "A finite-element formulation for sound field analyses with microperforated panel—Comparisons with electro-acoustical equivalent circuit theory and wave theory—," *Tech. Rep. Res. Comm. Archit. Acoust.*, AA2014-32, 6 pages (2014) (in Japanese).
- [4] T. Okuzono and K. Sakagami, "A finite-element formulation for room acoustics simulation with microperforated panel sound absorbing structures: Verification with electro-acoustical equivalent circuit theory and wave theory," *Appl. Acoust.*, **95**, 20–26 (2015).
- [5] K. Sakagami, M. Morimoto and M. Yairi, "A note on the effect of vibration of a microperforated panel on its sound absorption characteristics," *Acoust. Sci. & Tech.*, **26**, 204–207 (2005).
- [6] M. N. Guddati and B. Yue, "Modified integration rules for reducing dispersion error in finite element methods," *Comput. Methods Appl. Mech. Eng.*, **193**, 275–287 (2004).